# Bulk Coarse Particle Arching Phenomena in a Moving Bed with Fine Particle Presence

**Dawei Wang and Liang-Shih Fan**
Dept. of Chemical and Biomolecular Engineering, The Ohio State University, Columbus, OH 43210

*DOI 10.1002/aic.14320*
*Published online January 29, 2014 in Wiley Online Library (wileyonlinelibrary.com)*

*Bridging or arching of flowing solids particles is a serious hazard in the operation of moving bed systems. The mechanics of the arching has been extensively analyzed in the context of particle discharge from a hopper with conical geometry by considering the particulate layer stress distribution. However, bridging can also occur in a moving bed system with cylindrical geometry during the continuous mass flow of solids particles. Experimental work conducted in this study reveals that the appearance of solids bridging is normally accompanied by the presence of fine particles in the coarse moving particles as well as by the countercurrent interstitial gas flow. In this study, a stress analysis of the layered particles distributed in a cylindrical, vertical moving bed that flows downward opposing to upward flow of the interstitial gas is developed to quantify the bridging phenomenon. The analysis takes into account of the effects of presence of fine powder in the coarse particle flows and properties, such as particle-size distribution, bed voidage, and interstitial gas flow rate. The experimental validation of the present stress analysis for moving bed systems with varied fine and coarse particle concentration distributions, and interstitial gas velocities is also conducted. The stress distributions of the particles under flowing and arching conditions are obtained. An arching criterion is formulated, which indicates that the critical radius of the standpipe to avoid arching phenomenon is only related to the property of the bulk solids in the present geometric configuration of the flow system.* © 2014 American Institute of Chemical Engineers *AIChE J*, 60: 881–892, 2014

*Keywords: arching phenomenon, arching modeling, stress distribution, standpipe flow, critical bed size for arching, bed bridging, fine particle effects*

## Introduction

Granular materials in bulk are widely used in industrial systems. Processing of granular materials can be conducted in fluidized mode or nonfluidized mode. The fluidized mode is typically represented by fluidized beds as in bubbling bed, turbulent bed, and dense or dilute pneumatic conveying, while the nonfluidized bed mode is typically represented by fixed beds as in hoppers, bunkers, silos, and bins or by moving beds as in standpipes and diplegs. For nonfluidized bulk solids which are of interest in this study, they can support static shear stresses. Such a property yields a tendency of bridging or arching of bulk solids in nonfluidized mode transport. As can be seen in Figure 1, bridging or arching of bulk solids in reactors commonly associated with such system operational issues as solids agglomeration, local overheating, and formation of undesired reaction species. Bridging or arching of bulk solids caused by the presence of fine particles also occurs but is not well understood. It is, thus, necessary to examine the behavior of the fundamental stress properties of bulk solids in a moving bed condition, particularly when fine particles are present.

The problem of bridging of bulk solids in gravitational flow in silos is well known and extensively analyzed. As early as 19th century, the pressure distribution exerted by granular solids on the silo wall along the silo height was deduced by Janssen,[1] among others. Jenike derived systematic equations based on principles known in soil mechanics that describe stress distributions in silos and provide a guidance on designing the geometry of a mass flow silo including the angle and diameter of the silo outlet.[2,3] Following Jenike's studies, considerable research has been conducted both experimentally and analytically to ascertain their applications under different operational conditions as well as to enhance the accuracy of the equations by improving oversimplified assumptions in Jenike's analysis, which, in their original forms, ignored the possibility of an arch sliding along the hopper wall and the stresses on the top of the solid's layer.[4–8] As summarized by Nedderman et al.,[9] most studies have indicated no dependence of the particle discharge rate through the bottom nozzle on the height of the materials in the hopper and reported correlations relating the mass flow rate to the opening diameter and particle properties. Improved particle flowability of the hopper system has included injection of aeration gas near the hopper outlet.[10–12] Considerable studies using the computational technique to simulate the stress distribution for the granular flow through hopper outlet have also been carried out.[13–16]

Correspondence concerning this article should be addressed to D. Wang at wang.2744@osu.edu

**Figure 1. Photograph of arching.**

**[Color figure can be viewed in the online issue, which is available at wileyonlinelibrary.com.]**

Relatively little, in contrast, is reported on the arching phenomena of nonfluidized particles in vertical columns. Li studied the mechanism of arching in moving-bed standpipe with an interstitial gas flow from the particulate media mechanics. The study leads to the determination of a critical standpipe radius that is required to avoid arching as a function of particle properties and flow conditions.[17,18] However, arching phenomena can be significantly affected by the presence of the fine particles as well. Fine particles can be generated from attrition of the coarse particles in the operation of a fluidized bed when coarse particles are used. Therefore, the effect of the fine particles on the aching in a moving bed downcomer of coarse particles operated in a circulating fluidized bed system is required to be considered. Attrition could be attributed to mechanical and/or chemical stresses induced by particle–particle or particle–wall collision, thermal expansion, molar volume variation of reaction products in the course of circulating fluidized bed reactor operation. Thus, fine particles are present in a coarse particle flow system and their interactive effect on such flow properties as arching is inherent. Arching can cause serious operational hazard for a circulating fluidized bed reactor system. A typical example of such a system where arching can occur and needs to be avoided is the chemical looping reaction system for fossil fuel combustion or gasification.[19] A direct application of this study is, thus, the chemical looping reaction system.

Experiments conducted in a circulating fluidized bed system of coarse particles as shown in Figure 1 indicate the occurrence of solids bridging normally accompanied by the accumulation of fine powders in the coarse particles, and a change in the interstitial gas flow. The countercurrent interstitial gas flow to the solid flow provides an interphase drag thereby inducing opposing resistance that prevents a continuous downward solids flow driven by gravity. Thus, the change in the interstitial gas flow may yield stress redistribution in a layer of the coarse particles, causing interlocking of the particles and hence bridging formation. The accumulation of the fine powders will serve to alter the flow properties of the solids particles as well as to decrease the local voidage in the coarse particle moving bed. The latter may increase the interphase drag, whereas the former may alter the tendency of bridging for solids particles. It is important to ascertain the relationship between the tendency of bridging/arching and the flow properties under different operational conditions so as to provide proper actions to avoid bridging/arching occurrence. Included in this study is a theoretical stress analysis that is used to evaluate the tendency of arching/bridging of layered particles in a vertical moving standpipe with countercurrent interstitial gas flow. The analysis takes into account of the flow properties and characteristics of fine particles such as particle size, flowability, angle of repose, and unconfined yield stress. The effects of the particle size change, the volume fraction variation due to particle-size distributions, and the gas flow rate change on the tendency of bridging/arching are also studied. A validation of the present analysis is conducted with a simple experiment which is designed to measure the onset interstitial gas flow for forming an arch under the condition where a layer of fine particles is placed between coarse particles in a standpipe flow.

## Mechanistic Analysis and Experiments

When bulk solids are filled into a cylinder and loaded on top with a normal stress, $\sigma_1$, the bulk solid will be consolidated and compressed due to the effect of consolidation stress. If the bulk solid specimen prepared is then loaded with a vertical compressive stress, as shown in Figure 2, the bulk solid consolidates and the stress distributions inside the specimen can be described by the Mohr circle.[20] With the increasing of vertical load, the diameter of the Mohr circle increases correspondingly. When the Mohr circle is below the yield limit, as shown as $B_1$ and $B_2$, the bulk solid specimen only undergoes elastic deformation. The failure and/or incipient flow of bulk solids occur when the Mohr stress circle reaches to a critical value, given as circle $B_3$. The stress in the bulk solid specimen cannot exceed the yield limit, which is defined as unconfined yield strength. If at the same time, a horizontal stress, $\sigma_2$, is also exerted on the specimen, the specimen will consolidate (shown stress circle A). Until the stress circle touches the yield limit of the bulk solids (stress circle C), failure or incipient flow of bulk solids will occur. Thus, the yield limit is the envelope of all stress circles that indicate failure of a bulk solid sample.

The yield limit or the flowability of different bulk solids is different. The flowability of a bulk solids is normally characterized by the flow function, $ff_c$, which is defined as the ratio of consolidation stress, $\sigma_0$, used for preparing the specimen, to the unconfined yield strength, $f_c$ as given by

$$ff_c = \frac{\sigma_0}{f_c} \tag{1}$$

A larger flow function represents a better flowablity of bulk solids. Normally, the flow behavior of bulk solids can

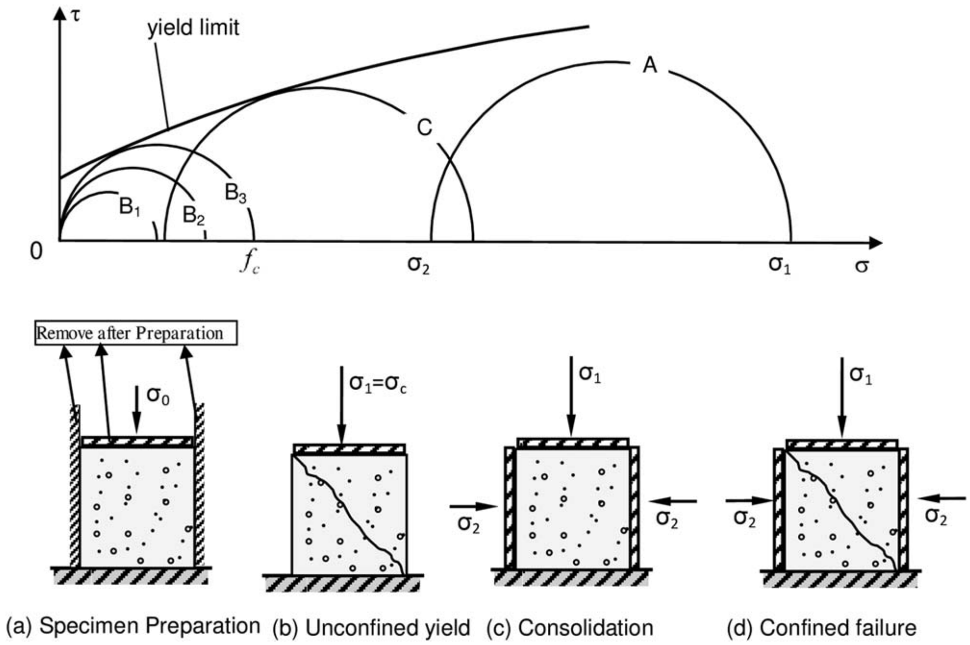


**Figure 2. Consolidation and yield process of a bulk solid specimen.[20]**

be classified as following according to Jenike as seen in Figure 3.[20]

$$\begin{cases} f_c < 1 & \text{not flowing} \\ 1 < ff_c < 2 & \text{very cohesive} \\ 2 < ff_c < 4 & \text{cohesive} \\ 4 < ff_c < 10 & \text{easy-flowing} \\ 10 < ff & \text{free-flowing} \end{cases}$$

### *Flowing solids in vertical cylindrical standpipe*

Consider a solid flowing in a vertical cylindrical standpipe. The bulk solids are assumed to be filled by layers, which consist of excentric circles with centers on the centerline of standpipe, as shown in Figure 4.

The two principal stresses exerted on any layer of bulk solids, $\sigma_1$ and $\sigma_2$, are assumed to be tangential and normal to the circle. Inside each layer of bulk solids, the two principal stresses are assumed to be uniform, which means the values of principal stresses are kept constant in the layer, although the directions will change along the circle. The continuous steady downward mass flow of bulk solids is due to the plastic deformation of each layer under the compression and shearing of stresses. Previous experiment data obtained for bulk solids showed that the major and the minor consolidating stresses during steady flow approaches to a constant value[2,3] as given by

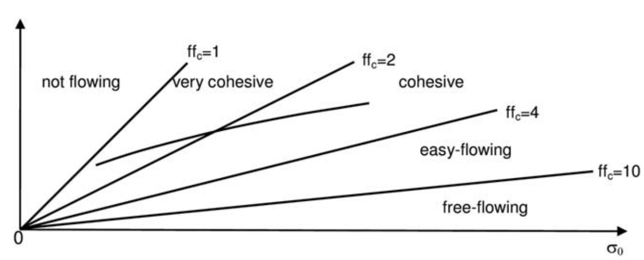


**Figure 3. Instantaneous flow function and lines of constant flowability.[20]**

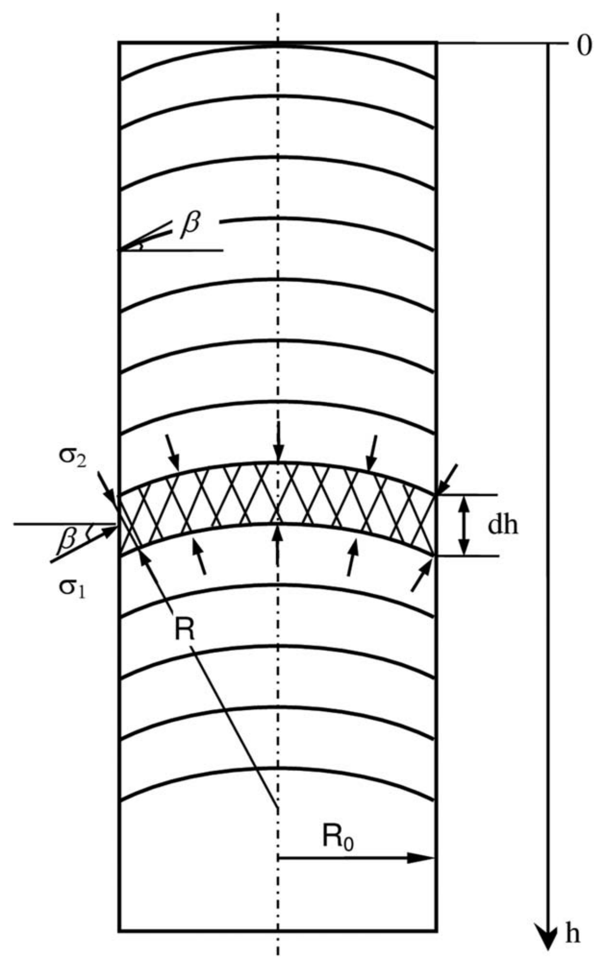


**Figure 4. Piles of bulk solids in cylindrical standpipe.**

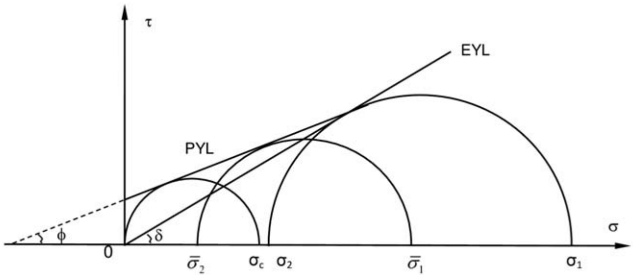


**Figure 5. Yield locus and principal stresses of bulk solids.**

$$\frac{\sigma_1}{\sigma_2}=\frac{1+\sin\delta}{1-\sin\delta} \tag{2}$$

where $\delta$ is a constant value determined only by material properties. The parameter is characterized by the effective angle of friction. The relationship of two principal stresses given by Eq. 2 represents a straight line named effective yield locus, passing through the origin with the inclined angle $\delta$ to the $\sigma$ axis, as shown in Figure 5. The effective yield locus is tangential to the Mohr stress circle of bulk solids to form an envelope determining the consolidating pressures during the mass flow.

Defining $\sigma=\frac{\sigma_1+\sigma_2}{2}$, the following equations can be easily obtained from relationships shown in Figure 5

$$\begin{cases}\sigma_x=\sigma(1+\sin\delta\cos 2\beta)\\ \sigma_y=\sigma(1-\sin\delta\cos 2\beta)\\ \tau_{xy}=\sigma\sin\delta\sin 2\beta\end{cases} \tag{3}$$

where $\beta$ is the angle between the direction of major principal stress and the direction perpendicular to the wall.

Although the above relationship has been known for a long time, it is not found to be applied on the stress analysis of flowing solids particles in a vertical moving bed standpipe. In the following section, the details of the derivation on the stress distribution of solids particles along the standpipe height by coupling the above relationship with the force balance equation are illustrated.

Under the condition of steady mass flow along the standpipe, the solids near the wall slide down on the wall and the frictional force on the solids from the wall can be expressed by

$$\tau_{xy}=\sigma_x\tan\varphi \tag{4}$$

where $\varphi$ is the angle of the friction between the powder and the wall.

Comparing Eqs. 3 and 4, the following equation can be obtained

$$\sin\delta\sin 2\beta=(1+\sin\delta\cos 2\beta)\tan\varphi \tag{5}$$

which gives

$$\sin(2\beta-\varphi)=\frac{\sin\varphi}{\sin\delta}=\sin v \tag{6}$$

Solving the above equation can give the angle between the major principal stress and the direction perpendicular to the wall, $\beta$. There are two solutions for $\beta$, which are located in the regions of [0, $\pi$/2] and [$\pi$/2,$\pi$], and are corresponding to the passive and active states of stress. The passive state of stress occurs during the filling of the pipe, while the active state of stress occurs during the discharging of bulk solids.

Under the condition of the steady mass flow rate, the bulk solids will be in a dynamic equilibrium state without any acceleration. The three forces act on each layer of the bulk solids, namely the gravity of the bulk solids, the net compressive force from the adjacent layers above and below, and the lift force from the wall, will balance with each other, which gives the following expression

$$\Delta W=\Delta F_1+\Delta F_c \tag{7}$$

where $\Delta W$ is the weight of the layer and is given by

$$\Delta W=\pi R_0^2\Delta h\rho_s g \tag{8}$$

$R_0$ is the radius of the standpipe; $\rho_s$ is the bulk density of the solids; $g$ is the gravity; and $\Delta h$ is the thickness of a layer of bulk solids.

The net lift force from the wall will be given by

$$\begin{aligned}\Delta F_1&=2\pi R_0\Delta h(\sigma_1\cos\beta\sin\beta-\sigma_2\sin\beta\cos\beta)\\&=\pi R_0\,\Delta h(\sigma_1-\sigma_2)\sin 2\beta\end{aligned} \tag{9}$$

The net compressing force from the adjacent layers of bulk solids can be written as

$$\Delta F_c=\pi R_0^2\Delta\sigma_2 \tag{10}$$

Putting Eqs. 8–10 into Eq. 7 and assuming $\Delta h\rightarrow 0$, a differential equation describing the stress change along the height of the standpipe can be obtained as

$$\rho_s g=\frac{2\sin\delta\sin 2\beta}{R_0(1-\sin\delta)}\sigma_2+\frac{d\sigma_2}{dh} \tag{11}$$

Solving the above differential equation gives the distribution of minor principal stress of bulk solids along the height of the standpipe as

$$\sigma_2=b+(\sigma_0-b)e^{-ah} \tag{12}$$

where the coefficients are

$$\begin{cases}a=\dfrac{2\sin\delta\sin 2\beta}{R_0(1-\sin\delta)}\\ b=\dfrac{R_0(1-\sin\delta)}{2\sin\delta\sin 2\beta}\rho_s g\end{cases} \tag{12a}$$

and $\sigma_0$ is the external minor principal stress exerted on top of the bulk solids in the standpipe.

It is noted that with the presence of the countercurrent interstitial gas flow, an additional upward drag force is exerted on the bulk solids. Assuming the gas flow is uniformly distributed and the particle distribution is homogeneous, the drag force, $F_D$, which normally can be expressed by the Ergun equation

$$F_D=150\frac{(1-\alpha)^2}{\alpha^3}\frac{\mu U}{d_p^2}+1.75\frac{(1-\alpha)}{\alpha^2}\frac{\rho U^2}{d_p} \tag{12b}$$

provides the same effect as the reduction of the solids weight. With a new parameter, apparent bulk density, $\rho_s'=\rho_s-F_D/g$ introduced, the stress distribution along the standpipe height can be expressed in the same form as Eq. 12 except that the coefficient b is redefined as

$$b=\frac{R_0(1-\sin\delta)}{2\sin d\sin 2\beta}\rho_s' g \tag{12c}$$

### *Arching solids in a vertical cylindrical standpipe*

To investigate the stress distribution when the solids is arching, a limiting case is considered, that is, when the solids are in transition from the flowing state to the arching state. Under this condition, the bulk solid is in a critical failure state of stress. As described in Section Flowing solids in vertical cylindrical standpipe, the stresses under the critical failure state can be described by a Mohr circle, which touches the yield line of the bulk solids. The incipient angle of yield line to the $\sigma$ axis, $\phi$, is noted as the angle of friction of the solids. It is observed that the angle of friction is not constant along the yield locus. However, the yield locus can be assumed to be a straight line as shown in Figure 5 when the major principal stress has a higher value. The assumption is supported by the data from shear cell tests with different solids, although it does not hold when the Mohr circle approaches the $\tau$ axis as the yield locus must bend downward and intercept the $\sigma$ axis at an angle of $\pi/2$.

From Figure 5, the relationship between the major and minor principal stresses, $\bar{\sigma}_1$ and $\bar{\sigma}_2$, is readily obtained as

$$\bar{\sigma}_1=f_c+\frac{1+\sin\phi}{1-\sin\phi}\bar{\sigma}_2 \tag{13}$$

The above known relationship reveals the general relationship of principal stresses in a specimen of bulk solids under a critical failure state of stress. By coupling it with the force balance equation of arched solids particles in a vertical standpipe, the stress distribution of solids' particles along the standpipe height can be obtained and analyzed.

Again, it is assumed that the bulk solids stored in the standpipe are in layers as illustrated in Figure 4. However, instead of the fully developed wall friction angle, which occurs in the mass flow state, the angle $\beta'$ of the solid layer intercepting the wall with respect to the direction perpendicular to the wall is more or less random as long as the net lift force provided by the wall can count-balance the downward force and prevent the solids from falling and/or sliding down. Here, considering the limiting case that the maximum lift force can be provided, one can find the critical angle from the following analysis.

The lifting force from the wall is related to the angle $\beta'$ by

$$\Delta F_l=\pi R\Delta h(\bar{\sigma}_1-\bar{\sigma}_2)\sin 2\beta' \tag{14}$$

The lift force will reach to the maximum when $\sin 2\beta'$ attains its maximum, which means $\beta'=\pi/4$. However, considering the limit of wall friction angle $\phi$, any value of angle $\beta'$ larger than $\phi$ means the solids will slide along the wall until the angle $\beta'$ is smaller than $\phi$. Thus, it yields

$$\beta'=\min(\phi,\pi/4) \tag{15}$$

Similar to the analysis in Section Flowing solids in vertical cylindrical standpipe, the differential equation for stress distribution along the standpipe height can be expressed as

$$\rho_s g=(\bar{\sigma}_1-\bar{\sigma}_2)\sin 2\beta'+\frac{d\bar{\sigma}_2}{dh} \tag{16}$$

With the aid of Eq. 13, the above differential equation can be solved as

$$\bar{\sigma}_2=b(1-e^{-ah})+\bar{\sigma}_0 e^{-ah} \tag{17}$$

where

$$\begin{cases} a=\dfrac{2\sin\phi\sin 2\beta'}{R_0(1-\sin\phi)} \\ b=\dfrac{R_0(1-\sin\phi)}{2\sin\phi\sin 2\beta'}\rho_s g-\dfrac{f_c(1-\sin\phi)}{2\sin\phi} \end{cases} \tag{17a}$$

$\bar{\sigma}_0$ is the external normal stress exerted on top of the bulk solids in the standpipe. If there is no external normal stress on top of the bulk solids, the equation can be reduced to

$$\bar{\sigma}_2=b(1-e^{-ah}) \tag{18}$$

Similar to the analysis in Section Flowing solids in vertical cylindrical standpipe, the presence of countercurrent interstitial gas flow can be treated as a reduction of the solids' weight by the interphase drag, $F_D$. The stress distribution in the solids maintains the same form as Eq. 17 with modified coefficient b as

$$b=\frac{R_0(1-\sin\phi)}{2\sin\phi\sin 2\beta'}\rho_s' g-\frac{f_c(1-\sin\phi)}{2\sin\phi} \tag{17b}$$

It should be noted that the above is a two-dimensional analysis that reveals the stress distribution of arched particles under a critical failure state of stress inside a vertical and cylindrical standpipe, taking into consideration the symmetry of the geometry and forces. In the case of inclined standpipes or standpipes in other shapes, a much more complicated nonsymmetric three-dimensional stress analysis in the standpipe has to be analyzed. With the standpipe inclined, the direction of gravity is no longer on the axis of the cylinder. The layers of bulk solids may not be assumed to be of excentric layers. The principal stresses on the layers of the bulk solids may not be tangential and normal to the circle. The stress condition at different points on the standpipe wall may be different. These factors greatly complicate the stress analysis.

### *Experimental validation*

There were no experimental results published for the flow and bridging of bulk solids in a vertical moving bed with fine powder and interstitial gas flow due to in part complexity of gas-solid flows. The complexity is also due to the fact that flow/arching criteria and pressure distribution are not only related to particle properties but also pipe geometries and the operational conditions. In this study, a simple experiment is designed to verify an application of the present analysis. The experiment investigates the occurrence of arching when a fine powder layer accumulates in between the coarse particles in a standpipe with varying interstitial gas flow.

Figure 6 shows the schematic diagram of the experimental setup. A clear plastic pipe with a diameter of 2.54 cm and a height of 0.9 m is used for the moving bed standpipe. A manual valve is installed at the bottom of the standpipe to control the solids flow rate. An airtight container connected to the bottom of the standpipe is used to store solids when the solids flow out of the standpipe. A gas inlet port is located on the side wall of the bottom section of the standpipe. A gas outlet port is located at the top section of the standpipe. The composite $Fe_2O_3$ particles with a diameter of 1.5 mm (coarse particles) are filled into the standpipe to form a section of a solids bed. A layer of fine particles of 300 μm is then placed above the bed of coarse solids. Another section of the same coarse particles is added on top of this layer of fine particles. The fine particle is a collection

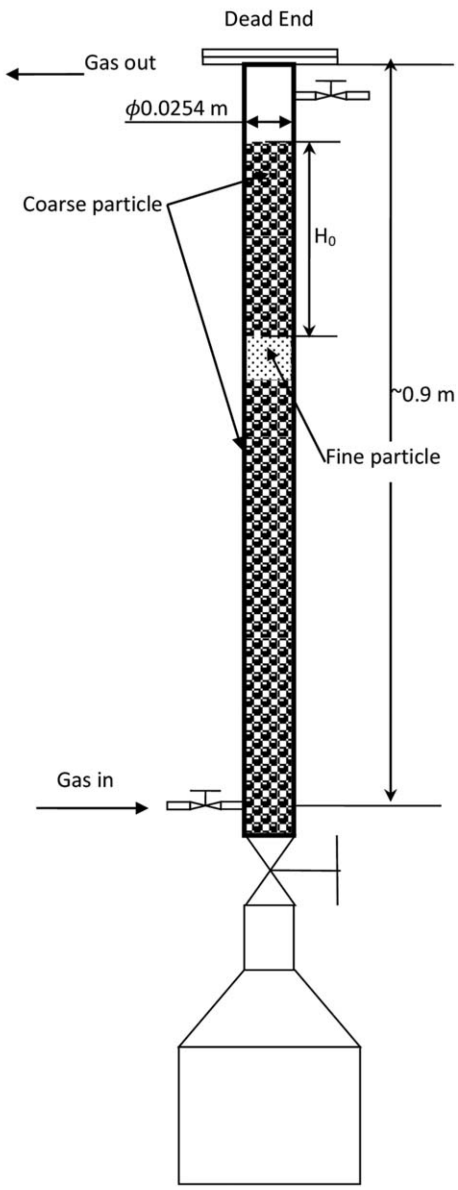


**Figure 6. Schematic diagram of experimental setup.**

of attrited coarse particles between the size range of 297–350 μm and has the same composition as the coarse particles. The effective angle of internal friction of the particles for both sizes is 21.5° as the angle is generally related to the type of materials used. When filling the fine particles to the top coarse particles, a special care has to be taken so that a minimal amount of fine particles falls into the bottom section of the coarse particles, despite the fact that the fallen fine particles do not affect the experimental result as the stress distribution in the bottom section of coarse particles does not affect the stress distribution in the layer of fine particles. After all the particles are filled into the standpipe, the heights of the fine particles and top section of coarse particles are recorded. During the experiments, the manual valve is partially open to discharge the particle at a steady rate. The interstitial gas flow is then provided. The gas flow rate is controlled by a flow meter and is gradually increased until the arching condition in the layer of fine particles is observed. The arching condition is reflected by the occurrence of discontinuity in the flow of fine particles. The value of the gas flow rate when the arching occurs is then recorded. The experiments indicate the relationship between the height of the layer of the fine particles and the apparent density of the particles under a certain amount of external force acting on the top of the fine particle layer. The variation of external force acting on the top of the fine particle layer in the parametric study of the experiment is obtained by changing the height of the top coarse particles as the stress at the dividing line between the top coarse particle and the fine particle layer can be related to the height of the top section of coarse particles using Eq. 17, given that the properties of coarse particles are known. Table 1 gives the results measured from the experiments, and the corresponding top external stress and apparent particle density obtained assuming the drag force can be calculated using Ergun equation. The comparison of the experimental results with the analytical predictions is given in Section Occurrence of fine powders.

It should be noted that the experiments are conducted in this study in a standpipe of a small diameter to substantiate the arching criterion developed. For experiments to be conducted at a larger standpipe diameter, to observe the arching phenomenon, it requires the size of fine particles to be decreased dramatically due to the relationship in which the required unconfined yield stress of the layer of fine particles increases with the column diameter according to Eq. 20. When the fine particle size substantially decreases, other factors such as particle-size distribution, gas flow uniformity, and consolidation condition of very fine particles may come

**Table 1. Experimental Data and Corresponding Conditions required for Arching**

| Case No. | Top Coarse Particle Height $H$ (cm) | Fine Powder Height $h$ (cm) | Predicted Gas Flow Rate $Q_g$ (scfh) | Actual Gas Flow Rate $Q_g$ (scfh) | Gas Superficial Velocity $u_g$ (m/s) | Top External Force (Pa) | Apparent Bulk Density $\rho_s$-$F_d/g$ (kg/m$^{3}$) |
|---|---|---|---|---|---|---|---|
| 1 | 5 | 3 | 2.25 | 2.37 | 0.037 | 348.76 | 896.84 |
| 2 | 5 | 4 | 1.25 | 1.44 | 0.022 | 353.12 | 1134.52 |
| 3 | 5 | 5 | 0.75 | 0.83 | 0.013 | 355.94 | 1291.79 |
| 4 | 7 | 3 | 2.68 | 2.89 | 0.045 | 394.92 | 763.88 |
| 5 | 7 | 4 | 1.56 | 1.65 | 0.026 | 401.67 | 1081.89 |
| 6 | 7 | 5 | 0.87 | 0.93 | 0.014 | 405.44 | 1265.64 |
| 7 | 10 | 3 | 3.12 | 3.30 | 0.051 | 429.26 | 657.03 |
| 8 | 10 | 4 | 1.75 | 1.86 | 0.029 | 437.97 | 1029.15 |
| 9 | 10 | 5 | 1.00 | 1.03 | 0.016 | 442.72 | 1239.47 |
| 10 | 15 | 3 | 3.12 | 3.10 | 0.048 | 451.61 | 710.51 |
| 11 | 15 | 4 | 1.81 | 1.86 | 0.029 | 459.41 | 1029.15 |
| 12 | 15 | 5 | 1.12 | 1.24 | 0.019 | 463.16 | 1187.05 |
| 13 | 15 | 6 | 0.62 | 0.72 | 0.011 | 466.21 | 1317.91 |

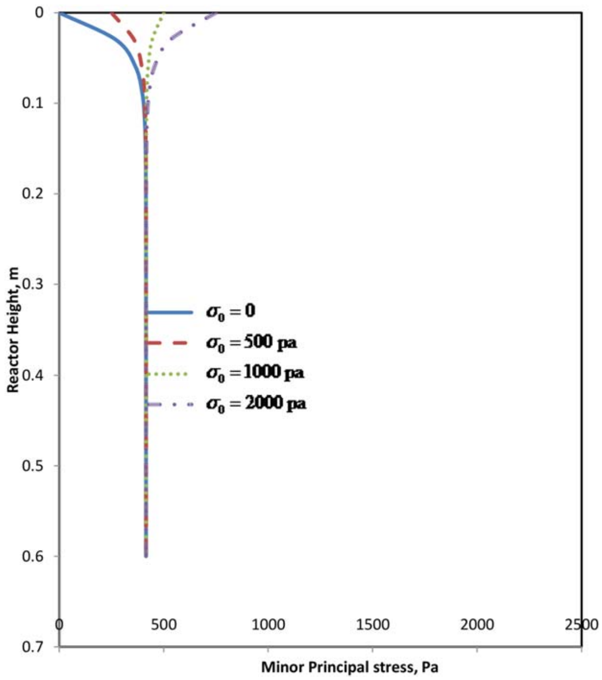


**Figure 7. Minor principal stress distribution of flowing bulk solids in standpipe with top external force.**

[Color figure can be viewed in the online issue, which is available at wileyonlinelibrary.com.]

into play in the practical analysis of this already complicate moving bed arching problem.

## Results and Discussion

The flow/arching criteria and pressure distribution of bulk solids in a vertical moving bed with fine powder and interstitial gas flow are not only related to the particle properties but also the pipe geometries and the operational conditions. In this section, the parametric studies of the flow conditions and stress distributions of different kinds of bulk solids are conducted. The comparison of the analytical results with the experiment results is also given.

### *Stress distribution in flowing powders*

From Eq. 12, it can be observed that the minor principal stress among flowing powders in a standpipe is an exponential function of the reactor height. The distribution of the minor principal stress is also determined by effective angle of friction, the angle between the direction of major principal stress and the direction perpendicular to the wall, the external minor principal stress exerted on top of the bulk solids, the solids bulk density, and the diameter of the standpipe.

As expressed in Eq. 12, the external stress at the top of the bulk solids has an effect on the stress distribution of the bulk solids along the reactor height. Figure 7 shows the minor principal stress distribution of the bulk solids along the reactor height under different external stresses at the top of the bulk solids. The bulk solids in the figure are assumed to have an effective angle of friction of 20°; the angle formed between the direction of major principal stress and the direction perpendicular to the wall by the bulk solids in the standpipe is 30°; The bulk density of the solids is 1500 kg/m$^3$; and the diameter of the standpipe is 2 in. As seen in Figure 7, when there is no external stress on the top of the bulk solids, that is, $\sigma_0=0$, the minor principal stress increases exponentially from zero at the top of the solids bed and approaches to a constant value after some distance away. It is noted that the application of the external force on the top of the bulk solids will only influence the stress distribution among the bulk solids in a relatively short distance.

Equation 12 also reveals that the minor principal stress increases with the increasing diameter of the standpipe, as given in Figure 8. It is understandable as the amount of the bulk solids proportionally increases with the cross-sectional area of the standpipe which increases faster than the diameter. It can, thus, be concluded that the wall of a standpipe with larger diameter sustains more stress than that of smaller diameter.

Figure 9 shows the minor principal stress distributions of bulk solids with different effective angle of internal friction. The maximum stress increases with the decreasing angle. It is noted that as a special case in which the effective angle of internal friction approaches to zero, it represents the property of liquid. The minor principal stress, which is the same as the major principal stress according to Eq. 2, equals the gravity of the bulk solids and represents the pressure of the liquid. This could partially prove the validity of the analysis. A similar relationship can also be found between the stress and twice the angle between bulk solids and the wall ($2\beta$), as seen in Figure 10.

### *Arching criteria*

The steady flow of bulk solids in the standpipe occurs only when the interparticle stress among bulk solids is big

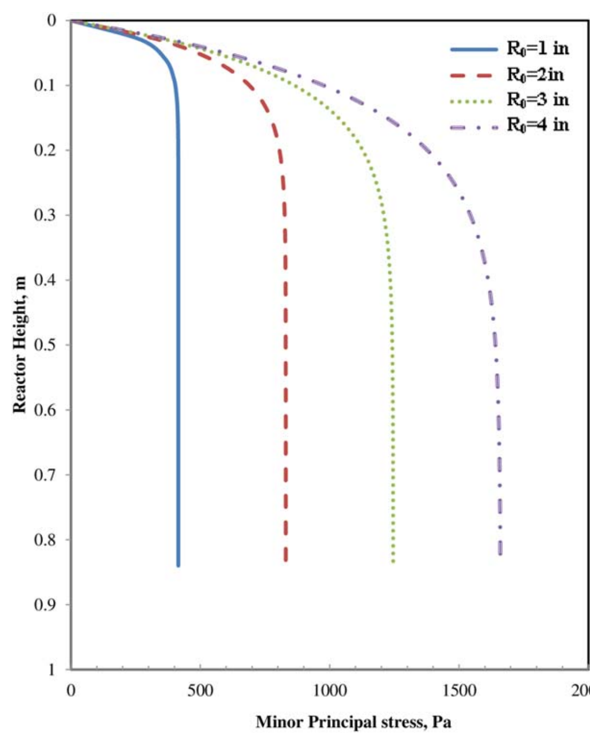


**Figure 8. Minor principal stress of flow bulk solids in standpipes with different radius.**

[Color figure can be viewed in the online issue, which is available at wileyonlinelibrary.com.]

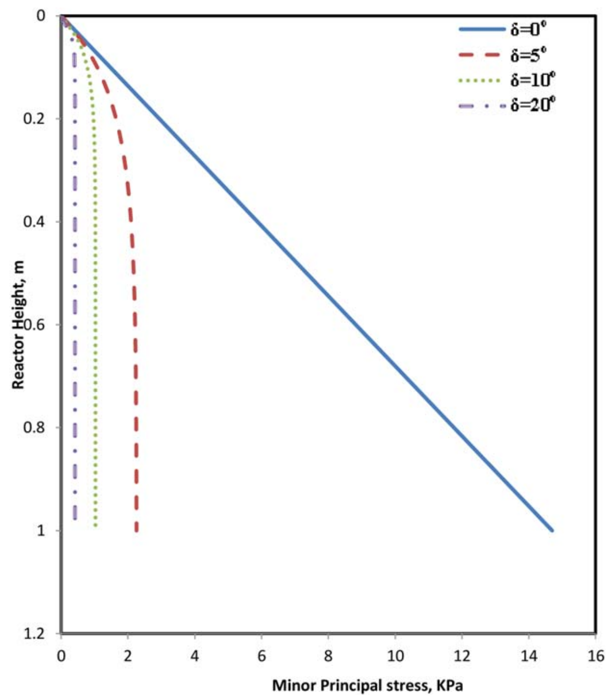


**Figure 9. Minor principal stress of flow bulk solids in standpipes with different effective angle of internal friction.**

**[Color figure can be viewed in the online issue, which is available at wileyonlinelibrary.com.]**

enough to exceed the static shear stresses that the nonfluidized bulk solids can support. When the interparticle stress is within the range that the bulk solids can sustain, bulk solids flow may transit to bridging or arching. From Section Arching solids in a vertical cylindrical standpipe, when an arch forms at a layer in the standpipe, the layer of bulk solids will sustain itself as well as the solids above this layer of bulk solids without the supporting force from the bottom solids. Thus, the minor principal stress on the bottom surface of the layer would be zero.

### *Minimum reactor diameter*

It can be concluded from Eq. 18 that with the absence of the top external force, the arch will form in the standpipe when coefficient $b$ reaches to zero, which gives

$$\frac{R_0(1-\sin\phi)}{2\sin\phi\sin2\beta'}\rho_s g=\frac{f_c(1-\sin\phi)}{2\sin\phi} \tag{19}$$

From this relationship, the critical, or minimum, radius of a cylindrical standpipe can be obtained as

$$R_0=\frac{f_c\sin2\beta'}{\rho_s g} \tag{20}$$

It can be seen that the critical radius is only related to the property of the bulk solids, that is, bulk density, unconfined yield stress, and the angle between solid layer and the wall. To avoid the arching of homogeneously distributed bulk solids, the practical size of the standpipe should be designed to be larger than the critical radius.

With the presence of the countercurrent interstitial gas flow, the new critical radius of the standpipe is then

$$R_0'=\frac{f_c\sin2\beta'}{\rho_s' g} \tag{21}$$

Comparing Eqs. 21 and 20, a conclusion can be drawn that the presence of the countercurrent interstitial gas flow increases the tendency of arching/bridging of bulk solids and, thus, a larger standpipe size is required, while a cocurrent interstitial gas flow is beneficial for the flowability of bulk solids in standpipe.

It should also be noted that in practice, the determination of critical radius of the standpipe is not as direct as the final form of Eq. 20 or 21 indicates as the unconfined yield stress and bulk density are not the intrinsic properties of solids materials. Rather, they are influenced by a number of such variables as particle-size distribution, particle shape, moisture level, and packing condition. Detailed discussion on the effects of these variables is given in following sections.

### *External force to break arch*

When a change in the bulk solids property and/or an increase in the gas flow rate lead to the failure in a standpipe flow, it indicates that the coefficient $b$ in Eq. 17 is less than zero. From the equation, it can be noted that exerting an external normal stress on the top of solids can keep the minor principal stress larger than zero so as to prevent the occurrence of arching. By letting the value be equal to zero, a minimum external normal stress can be obtained as

$$\bar{\sigma}_0=-b\left(\frac{1}{e^{-ah}}-1\right) \tag{22}$$

It can be seen from the equation that the required external normal stress for solids failure increases with the total height of solids in the standpipe.

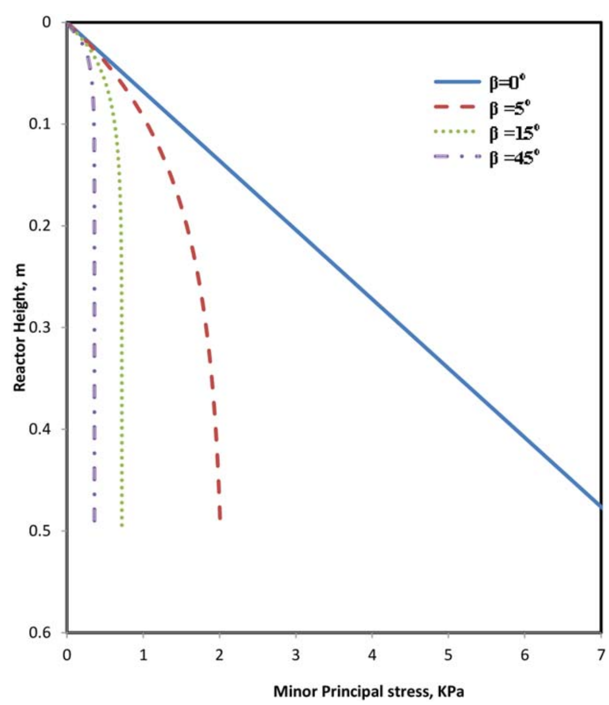


**Figure 10. Minor principal stress of flow bulk solids in standpipes with different angle between solids layer and wall.**

**[Color figure can be viewed in the online issue, which is available at wileyonlinelibrary.com.]**

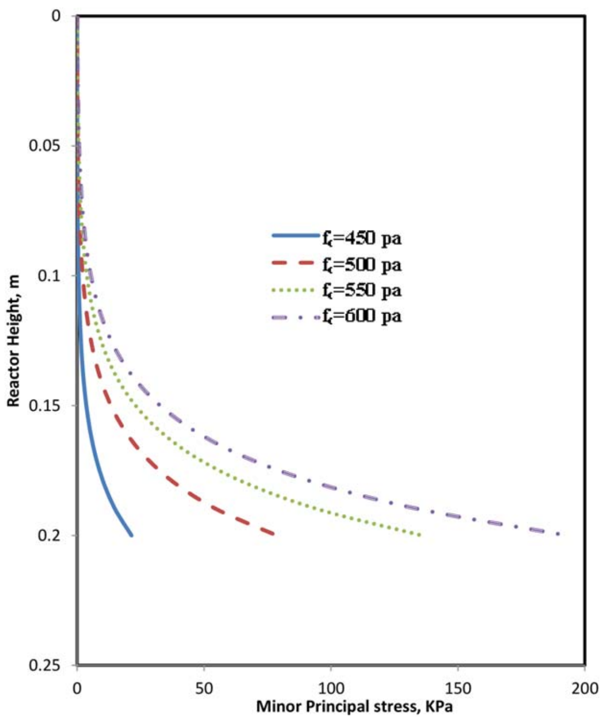


**Figure 11. Required top external force to avoid arching of bulk solids with different unconfined yield stress.**

[Color figure can be viewed in the online issue, which is available at wileyonlinelibrary.com.]

Figure 11 shows the external force needed to break an arch formed by bulk solids for different unconfined yield stresses. It can be seen that the external force needed increases dramatically with the increasing unconfined yield stress. The parameters used in the calculation are given in Table 2.

### *Influence of the particle size*

The flowability or the tendency to arching of bulk solids is directly related to the unconfined yield stress. It is due to the existance of the unconfined yield stress in the bulk solids that the layer of bulk solids can maintain the stress holding material on a free surface and resist external forces that attempt to break the surface. The unconfined yield stress of bulk solids accounts for the interparticle forces in the overlapping layers of the particles. Several models with different mechanisms proposed to quantify the unconfined yield strength are given in Table 3. All of them conclude that the unconfined yield strength is inversely proportional to a power function of the particle diameter. Previously published experimental data also confirmed the relationship. For example, the unconfined yield strength of some alumina powders with different particle sizes were measured by Kohler and Schubert,[25] as shown in Figure 12. The moisture content in the bulk solids in the experiments is about 0.2% wt. It is seen that the unconfined yield strength of the alumina powders increases dramatically with decreasing powder sizes.

**Table 2. Parameters used in Theoretical Analysis**

| Parameter | Symbol | Value | Unit |
|---|---|---|---|
| Solids bulk density | $\rho_s$ | 1500 | (kg/m$^3$) |
| Effective angle of internal friction | $\delta$ | 20 | o |
| Angle between solids layer and wall | $\beta'$ | 30 | o |
| Standpipe diameter | $D_0$ | 0.0254 | (m) |

**Table 3. Relationship Between Unconfined Yield Strength and Particle Size**

| Model | Mechanism | Source |
|---|---|---|
| $f_c = \frac{K_1}{D_p^2}$ | Van der Waals forces | Mollerus[21] |
| $f_c = \frac{K_2 \cdot \sqrt{C}}{D_P}$ | Capillary forces | Rabinovich[22] |
| $f_c = \frac{K_3}{D_p^{0.5}}$ | Elastic fracture | Rumpf[23] |
| $f_c = \frac{K_4}{D_p^n}$ | Plastic-elastic fracture | Specht[24] |

With the relationship between the unconfined yield strength and the particle size, the relationship between the critical reactor diameter and the particle size can be obtained using Eq. 20. Figure 13 exemplified such a relationship using the experimental data at a major consolidation stress of 10 kPa in Figure 12. Due to the dramatic increase in the unconfined yield stress, the critical reactor diameter for small size of powders is significantly larger than that for large size of powders.

### *Influence of fine powder mixing in coarse particles*

It should be noted that the above analysis is based on spherical particles of uniform particle size. The flowability of bulk solids containing a mixture of powders with different sizes is invariably affected by the presence of the fines fraction. This can be explained by the fact that the shearing and bonding of the bulk solids take place across the contact points of the particles. The fine powders provide more contact points than do coarse particles. The effects of the interparticle forces among fine powders are also greatly larger than those among coarse particles. The mixing of fine powders with coarse particles decreases the voidage of the bulk solids. This will also significantly increase the drag force at the occurrence of interstitial gas flow and, thus, decrease the flowability of bulk solids.

### *Occurrence of fine powders*

The flowability of the bulk solids decreases due to the increased unconfined yield stress of the particles when a layer of fine powders is present in the standpipe. An arch

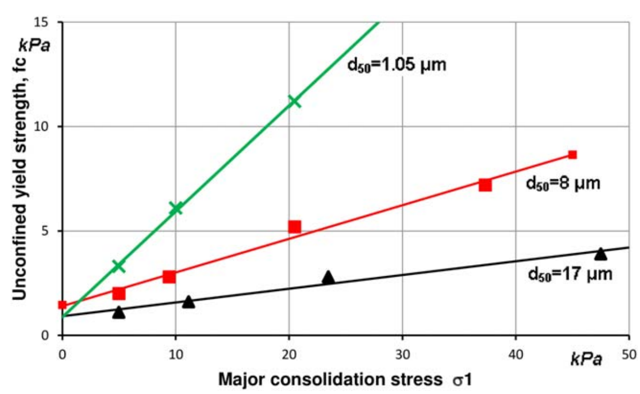


**Figure 12. Experimental data of unconfined yield strength of some alumina-powders with different particle sizes.[25]**

[Color figure can be viewed in the online issue, which is available at wileyonlinelibrary.com.]

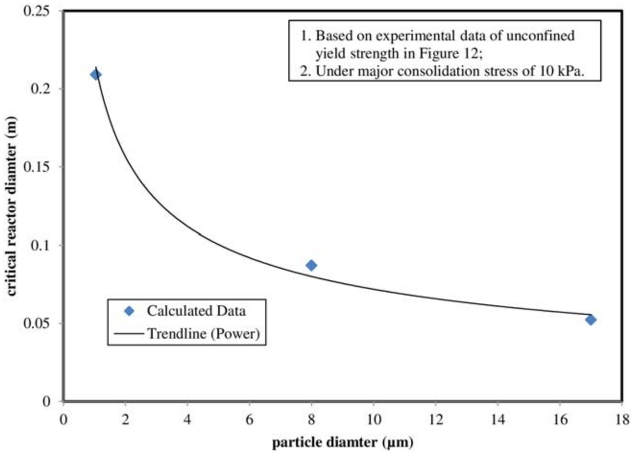


**Figure 13. Critical reactor diamter for bulk solids with different particle size.**

[Color figure can be viewed in the online issue, which is available at wileyonlinelibrary.com.]

may or may not form depending on the stress exerted from larger particles on top of the fine powder layer, the thickness of the layer, and the properties of the fine powders. Assume that coarse particles are uniformly distributed with a height of $H_0$ on top of the layer of fine powders as shown in Figure 14. The stress on top of the fine powder layer can be treated

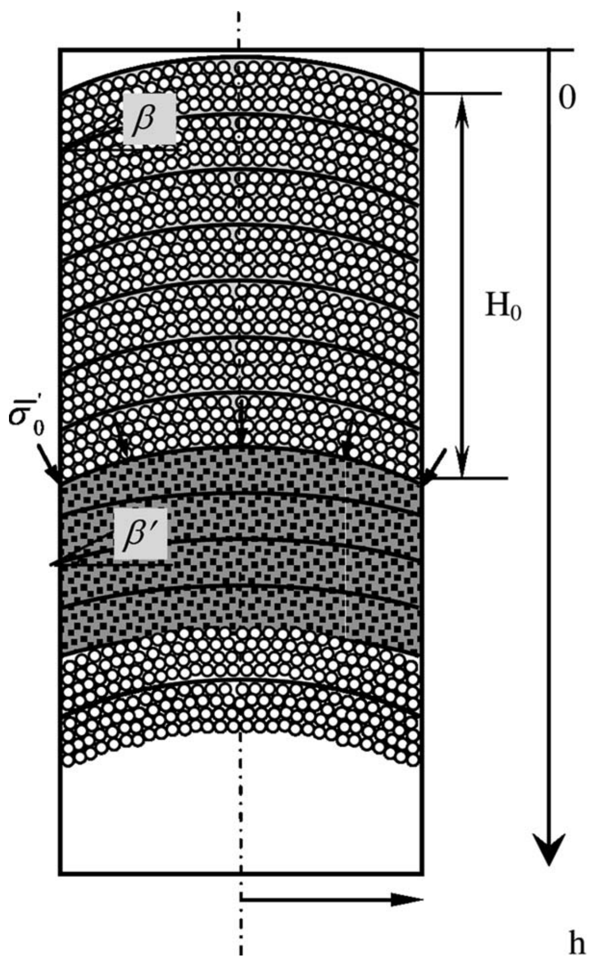


**Figure 14. Standpipe flow with the presence of a fine powder layer between bulk coarse solids.**

as external stress, which can be given in the following equation according to the analysis in Section Mechanistic Analysis and Experiments

$$\bar{\sigma}_0' = \bar{\sigma}_{2H} = b(1 - e^{-aH_0}) \tag{23}$$

The minor principal stress distribution along the height of the fine powder layer can be obtained by

$$\bar{\sigma}_2' = b_f(1 - e^{-a_f h}) + \bar{\sigma}_0' e^{-a_f h} \tag{24}$$

where the values of coefficients $a_f$ and $b_f$ are determined by the properties of the fine powders.

The aching occurs at a location where its minor principal stress reaches zero. Based on it, the critical thickness of the fine powder layer, that is, minimum height to form an arch, can be obtained as

$$h = -\frac{1}{a_f} \ln \frac{b_f}{b_f - \bar{\sigma}_0'}, \tag{25}$$

The minimum height, $h$ decreases when $b_f$ increases and/or $\bar{\sigma}_0'$ decreases. It should be noted that Eq. 25 is meaningful only when $b_f < 0$, which means the occurrence of arching is possible.

Figure 15 shows the relationship between the critical thickness of the fine powder layer and the apparent bulk density of the bulk solids. It is found that with the increasing of the apparent bulk density, through the actual increasing of bulk density of solids and/or the decreasing of drag force, the critical thickness of the fine powder layer will increase. This means that the influence of the fine powder layer on the flowability of bulk solids is less for particles with higher densities or with less drag forces. It is also found that the higher the top external force is, the larger critical fine powder layer thickness will be.

Figure 16 shows the experimental results from Section Experimental validation and their comparison with the analytical prediction. The unconfined yield stress of the fine particles can be obtained by translational shear tester based on Jenike's theory,[20] In this article, however, a value of 600 Pa, which is extrapolated based on the obtained experimental

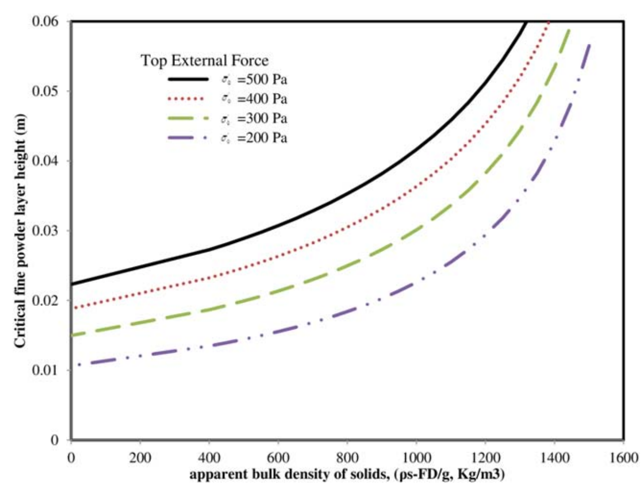


**Figure 15. Critical fine power thickness with different apparent bulk density under different top external pressure.**

[Color figure can be viewed in the online issue, which is available at wileyonlinelibrary.com.]

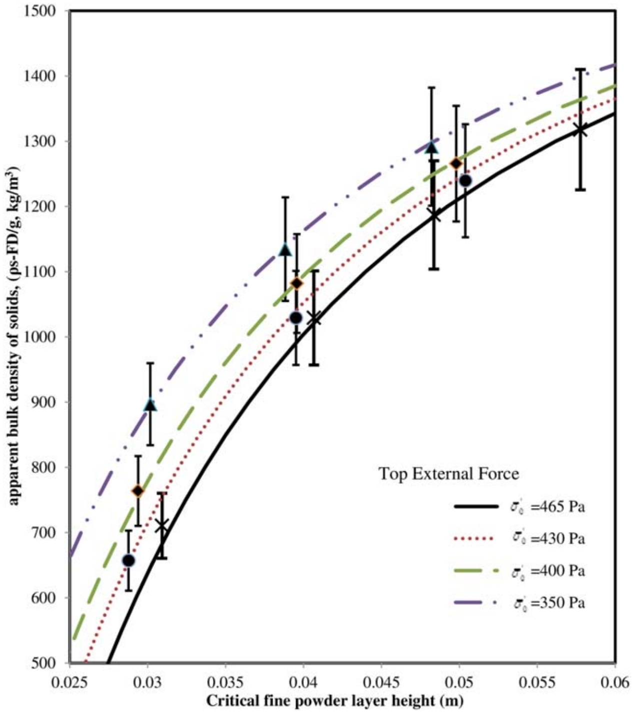


**Figure 16. Experimental validation on the relationship between critical fine powder layer height and apparent bulk density solids under different top external forces.**

[Color figure can be viewed in the online issue, which is available at wileyonlinelibrary.com.]

data, is used for the analysis. It is found that under different top external forces, the analytical prediction on the relationship between the critical fine powder layer thickness and its apparent density matches the experimental data very well. The slightly higher actual air flow rate used than the predicted flow rate on the arching formation (as shown in Table 1) is possibly due to the error induced in the measurements and predictions of the unconfined yield stress, the effective angle of internal friction, the influence of particle-size distribution, and the interpenetration between the coarse particle and the fine powder layer. The stability of experimental conditions, such as the gas flow rate, consolidation of solids particles, also has significant influence on the experimental results. The instability of the gas flow rate causes the instability of the stresses among the solids particles and may cause the solids particle to deviate from the critical failure status. The consolidation of the solids particles may greatly alter the unconfined yield stress of the solids particles, leading to different experimental results. With special attention on the stability issue by minimizing the consolidation of solids particles and the fluctuation of gas flow, repeated experiments under different conditions were performed yielding results in a range of deviation of $\pm$ 7% and proving reliable experimental results.

## Concluding Remarks

In this study, a mechanistic analysis of flow and bridging of bulk coarse particles in a vertical moving bed with interstitial gas flow and with fine particle presence is conducted to describe the solids flow condition and the coarse particle bridging phenomenon. The analysis relates the flowability and arching criteria to pertinent intrinsic characteristics of bulk solids including effective angle of internal friction of bulk solids, arching angle between solids layer and wall, unconfined yield stress of bulk solids, bulk solids density, and such operational conditions as standpipe diameter and drag force due to interstitial gas flow. The analysis provides the stress distributions of moving bed particles along the height of the standpipes under various operational conditions. The arching criterion for the bulk solids is also obtained from this analysis. The critical standpipe diameter to avoid arching in the standpipe for specific properties of bulk solids is given. The effects of external force, particle size, and extent of fine particle presence on the occurrence of arching are also illustrated. A simple experiment is performed to substantiate the mechanistic analysis of this study.

## Notation

$F_D$ = drag force
$\Delta F_1$ = net lift force from the wall
$\Delta F_c$ = net compressing force from the adjacent layers of bulk solids
$f_c$ = unconfined yield strength
$ff_c$ = flow function
$g$ = gravitational acceleration
$h$ = the minimum height to form arch
$\Delta h$ = thickness of a layer of bulk solids
$R_0$ = standpipe diameter
$\Delta W$ = weight of solids layer
$\beta$ = angle between solids layer and the direction perpendicular to the wall
$\beta'$ = angle between arched solid layer and the direction perpendicular to the wall
$\phi$ = angle of the friction between powder and wall
$\delta$ = effective angle of friction
$\rho_s'$ = solids bulk density
$\rho_s'$ = apparent bulk density
$\sigma_0$ = external stress exerted on top of the bulk solids
$\bar{\sigma}_0$ = external stress exerted on top of arched bulk solids
$\sigma_1$ = principal stresses tangential to the circle
$\sigma_2$ = principal stresses normal to the circle
$\bar{\sigma}_1$ = major principal stress under arching condition
$\bar{\sigma}_2$ = minor principal stress under arching condition
$\sigma_x$ = normal stress in x-direction
$\sigma_y$ = normal stress in y-direction
$\tau_{xy}$ = shear stress in x-y coordinate

## Literature Cited


1. Sperl M. Experiments on corn pressure in silo cells—translation and comment of Janssen's paper from 1895. *Granular Matter*. 2006;8(2): 59–65.
2. Jenike AW. Gravity Flow of Bulk Solids. Vol. Bulletin 108. Utah: Utah University, 1961.
3. Jenike AW. Storage and Flow of Soloids. Vol. Bulletin 123. Utah: Utah University, 1964.
4. Eckhoff RK, Leversen PG. A further contribution to evaluation of jenike method for design of mass flow hoppers. *Powder Technol*. 1974;10(1–2):51–58.
5. Enstad G. Theory of arching in mass flow hoppers. *Chem Eng Sci*. 1975;30(10):1273–1283.
6. Walters JK. Theoretical analysis of stresses in axially-symmetric hoppers and bunkers. *Chem Eng Sci*. 1973;28(3):779–789.
7. Walters JK. Theoretical analysis of stresses in silos with vertical walls. *Chem Eng Sci*. 1973;28(1):13–21.
8. Wright H. *An Evaluation of the Jenike Bunker Design Method*. Journal of Engineering for Industry. 1973;95(1): p. 48–54.
9. Nedderman RM, Tüzün U, Savage SB, Houlsby GT. The flow of granular-materials I. Discharge rates from hoppers. *Chem Eng Sci*. 1982;37(11):1597–1609.
10. Huang WJ, Gong X, Guo XL, Dai ZH, Liu HF, Zheng LJ, Zhao JC, Xiong YJ. Discharge characteristics of cohesive fine coal from aerated hopper. *Powder Technol*. 2009;194(1–2):126–131.

11. Johanson K. Rathole stability analysis for aerated powder materials. *Powder Technol.* 2004;141(1–2):161–170.
12. Ouwerkerk CED, Molenaar HJ, Frank MJW. Aerated bunker discharge of fine dilating powders. *Powder Technol.* 1992;72(3):241–253.
13. Langston PA, Tuzun U, Heyes DM. Discrete element simulation of granular flow in 2d and 3d hoppers—dependence of discharge rate and wall stress on particle interactions. *Chem Eng Sci.* 1995;50(6): 967–987.
14. Potapov AV, Campbell CS. Computer simulation of hopper flow. *Phys Fluids.* 1996;8(11):2884–2894.
15. Matchett AJ. Stresses in a bulk solid in a cylindrical silo, including an analysis of ratholes and an interpretation of rathole stability criteria. *Chem Eng Sci.* 2006;61(6):2035–2047.
16. Datta A, Mishra BK, Das SP, Sahu A. A DEM analysis of flow characteristics of noncohesive particles in hopper. *Mater Manuf Process.* 2008;23(2):196–203.
17. Li HZ. The dynamics of nonfluidized gas-particle flow. *Powder Technol.* 1992;73(2):147–156.
18. Li HZ. Mechanics of arching in a moving-bed standpipe with interstitial gas-flow. *Powder Technol.* 1994;78(2):179–187.
19. Fan LS. Chemical Looping Systems for Fossil Energy Conversions. Wiley-AIChE, Hoboken, NJ, 2010.
20. Schulze D. *Powders* and Bul Solids. New York: Springer Berlin Heidelberg, 2008:352.
21. Molerus O. The role of science in particle technology. *Powder Technol.* 2002;122:156–167.
22. Rabinovich Y, Esayanur MS, Johanson K, Moudgil B. Oil Mediated Particulate Adhesion and Mechanical Properties of Powder. *Proceedings of the World Congress on Particle Technology*. Sydney, Australia, 2002.
23. Rumpf H. Particle Technology. New York: Chapman and Hall, 1990.
24. Specht D. Caking of Granular Materials: an Experimental and Theoretical Study, PhD Thesis. Florida: University of Florida, 2006.
25. Kohler T, Schubert H. Influence of the particle-size distribution on the flow behavior of fine powders. *Part Part Syst Charact.* 1991; 8(2):101–104.

*Manuscript received Jan. 22, 2013, revision received Sept. 3, 2013, and final revision received Dec. 6, 2013.*